How wind shear affects trade-wind cumulus convection

K. C. Helfer[1], L. Nuijens[1], S. R. de Roode[1], A. P. Siebesma[1,2]

[1]Department of Geoscience and Remote Sensing, Delft University of Technology, Delft, The Netherlands
[2]Royal Netherlands Meteorological Institute (KNMI), De Bilt, The Netherlands

Key Points:

- Shear in the zonal wind influences cloud top heights via the effect of momentum transport on the surface wind and surface fluxes.
- Backward shear (surface easterlies turn westerlies) lowers cloud tops and shallows and moistens the trade-wind layer.
- Any absolute amount of wind shear limits in-cloud updraft speeds and enhances low-level cloud fraction.

Corresponding author: Kevin Helfer, k.c.helfer@tudelft.nl

Abstract

Motivated by an observed relationship between marine low cloud cover and surface wind speed, this study investigates how wind shear affects shallow cumulus convection. We ran large-eddy simulations for an idealised case of trade-wind convection using different vertical shears in the zonal wind. Backward shear, whereby surface easterlies become upper westerlies, is effective at limiting vertical cloud development, which leads to a moister, shallower and cloudier trade-wind layer. Without shear or with forward shear, shallow convection tends to deepens more, but clouds tops are still limited under forward shear. A number of mechanisms explain the observed behaviour: First, shear leads to different surface wind speeds and, in turn, surface heat and moisture fluxes due to momentum transport, whereby the weakest surface wind speeds develop under backward shear. Second, a forward shear profile in the subcloud layer enhances moisture aggregation and leads to larger cloud clusters, but only on large domains that generally support cloud organization. Third, any absolute amount of shear across the cloud layer limits updraft speeds by enhancing the downward-oriented pressure perturbation force. Backward shear — the most typical shear found in the winter trades — can thus be argued a key ingredient at setting the typical structure of the trade-wind layer.

Plain Language Summary

We used a high-resolution weather model to investigate the influence of the shape of the wind profile (i.e. whether the wind blows faster, slower or with the same velocity at greater altitudes compared to the surface) on shallow cumulus clouds typical of the North Atlantic trade-wind region. In this region, easterly winds that decrease with height (and eventually turn westerly) are most common. Generally, the surface winds are also affected by how the wind blows further aloft, influencing what kind of clouds form. But even when we eliminate this effect in our study, we find that when the wind blows faster or slower at greater heights, clouds are not only tilted but also wider, and both effects increase the overall cloud cover. Furthermore, if the wind speed changes with height, the updraft speed within clouds is diminished, which potentially decreases the height of clouds. However, if the wind speed increases with height (which only rarely occurs in the trades), clouds tend to cluster more, which 'offsets' the weaker updrafts, and thus still allows for deeper clouds.

1 Introduction

In light of the uncertain role of trade-wind cumulus clouds in setting the cloud feedback, there is widespread interest in understanding the behaviour of these clouds, the different ways they interact with their environment and how this changes in response to warming (e.g. Bony & Dufresne, 2005; Bony et al., 2013; Vial et al., 2017). Trade-wind cumuli are found in regions characterised by the trade winds, yet we understand relatively little about how they depend on the structure of the trade wind, compared to how they depend on temperature and moisture. Some studies have investigated the influence of the wind speed on low clouds in the trades and revealed that wind speed is one of the better predictors of low cloud amount (e.g. Nuijens & Stevens, 2012; Brueck et al., 2015; Klein et al., 2017). But it is unclear how much the wind shear itself plays a role in observed cloud amount–wind speed relationships, as one might expect both wind speed and wind shear to increase with larger meridional temperature gradients throughout the lower troposphere when assuming geostrophic and thermal wind balance. Furthermore, little work has concentrated on the influence of wind shear on convection, other than its role in increasing the amount of projected cloud cover.

From studies of deep convection we know that wind shear can have a number of effects. Shear is effective at organizing deep convective systems into rain bands and squall lines (e.g. Thorpe et al., 1982; Rotunno et al., 1988; D. J. Parker, 1996; Hildebrand, 1998; Robe & Emanuel, 2001; Weisman & Rotunno, 2004). At the same time, shear can limit convection during its developing stages (Pastushkov, 1975). A recent paper by Peters et al. (2019) clearly shows how shear reduces updraft speeds in slanted thermals by enhancing the (downward-oriented) pressure perturbations. Shear is also argued to inhibit deep convection by 'blowing off' cloud tops (e.g. Sathiyamoorthy et al., 2004; Koren et al., 2010), which we interpret as an increase in the cloud surface area that experiences entrainment, which also plays a role in setting updraft buoyancy and updraft speeds.

Malkus (1949) might have been one of the first to mention the effect of shear on shallow convection, noting that the tilting of clouds through shear causes an asymmetry in its turbulence structure with more turbulence on the windward than the leeward side. Through numerous studies we now know that shear helps organize shallow convective clouds in rolls or streets along with the development of coherent moisture and temperature structures in the subcloud layer (e.g. Malkus, 1963; Hill, 1968; Asai, 1970; LeMone

& Pennell, 1976; Park et al., 2018). Li et al. (2014) explain how shear over the subcloud layer interacts with the low-level circulation induced by cold pools to enhance or limit the regeneration of convective cells and longevity of shallow cloud systems. Brown (1999) shows that shear can strongly affect the surface wind via momentum transport, but that it has little effect on the turbulence kinetic energy (TKE) budget, on scalar fluxes and on cloud properties. This is in contrast to the dry convective boundary layer, where shear has a strong impact on the TKE budget (Fedorovich & Conzemius, 2008, and references therein).

The present study asks how wind shear influences trade-wind cumulus convection, cloud amount and the structure of the boundary layer. To this end, we used an idealised large-eddy-simulation (LES) framework — inspired by Bellon and Stevens (2012) and Vogel et al. (2016) and not unlike the typical atmosphere in the trades — aiming at a fundamental understanding of the sensitivity to forward and backward shear (by which we mean an increase and decrease, respectively, of the zonal wind speed with height) of different strengths.

The remainder of this paper is structured as follows. We first explain our idealised LES set-up and the wind shear variations we impose. The results are then presented in a twofold manner. First, we discuss the effects of shear on the cloud and boundary layer evolution, showing results from large- and small-domain simulations with interactive and prescribed surface fluxes. Second, focusing on the large-domain runs with constant surface fluxes, we discuss how shear impacts the cloud structure and cloud depth without surface flux responses. We end with a concluding discussion and an outlook on future work. In an appendix, we discuss the influence of shear on the clouds' vertical velocity budget.

2 Experimental design

We carried out large-eddy simulations (LES) using version 4.2 of the Dutch Atmospheric Large Eddy Simulation (DALES; Heus et al., 2010). In our experimental set-up, we prescribed large-scale forcings and initial profiles typical of the North Atlantic trades at a latitude of $\varphi = 15°$ N. The standard case set-up is inspired by that of Vogel et al. (2016) and Bellon and Stevens (2012), who introduced an idealised modeling framework with only a limited set of parameters that represent the large-scale flow. The initial tem-

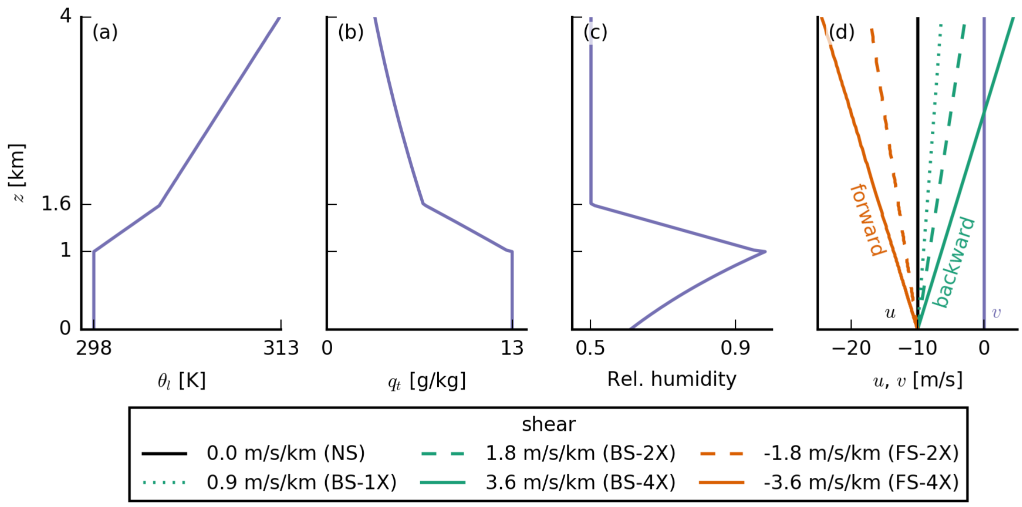

Figure 1. Initial profiles of (a) the liquid water potential temperature θ_l, (b) total water specific humidity q_t, (c) relative humidity and (d) the two wind components u and v. Purple profiles are the same in all simulations. Orange stands for forward shear (FS) and green for backward shear (BS). Same line types indicate the same amounts of absolute shear (1X, 2X, 4X). The colour coding of the different shears is the same for all other figures.

perature and humidity profiles of our simulations (Fig. 1) have a well-mixed layer of 1 km depth over a surface with a constant sea-surface temperature (SST) of 300 K. The mixed layer is topped by a 600-m-deep inversion layer. In the free troposphere, the profile of liquid water potential temperature θ_l follows a constant lapse rate of 4 K/km, and the relative humidity is constant with height at 50 percent. We applied a constant radiative cooling rate of -2.5 K/d to θ_l, which promotes relatively strong shallow convection, allowing for the development of the congestus clouds we are interested in. We increased the domain top to 18 km to allow for deeper convection. Between 10 and 18 km, the radiative cooling is quadratically reduced to zero. The relative humidity reaches 0 at about 14 km, which is also the lower boundary of the sponge layer in our LES. The θ_l lapse rate above 10 km is 8 K/km reflecting a stable upper atmosphere. In all simulations, we used a single-moment ice microphysics scheme (Grabowski, 1998) and allowed for precipitation assuming a constant cloud droplet concentration of 60 cm^{-3}.

Different than Vogel et al. (2016), we used a weak temperature gradient (WTG) assumption to calculate the subsidence profile, as the deeper congestus clouds that develop increasingly violate the assumption of a strongly subsiding atmosphere. Practically,

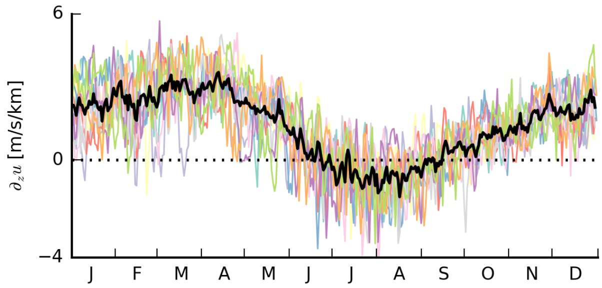

Figure 2. Time series of the amount of zonal shear between 1 and 3 km for the years 2008 to 2017 averaged over the area from 9° to 19° N and from 50° to 59° W (coloured lines). The black line is the average over all 10 years. The dotted horizontal line indicates 0 m/(s km). Data are from the ERA5 reanalysis.

the WTG method was implemented following Daleu et al. (2012): Above a reference height, we calculated the subsidence rate w_s such that it maintains the virtual potential temperature θ_v close to its initial (reference) profile $\theta_{v,0}$ according to

$$w_s = \frac{1}{\tau}\frac{\overline{\theta_v} - \theta_{v,0}}{\partial_z \theta_{v,0}}, \tag{1}$$

where the overbar indicates slab averaging, ∂_z symbolizes the vertical derivative and τ is the relaxation time scale, which was set to 1 h. WTG is not valid at levels where turbulence and convection effectively diffuse gravity waves. We define this level to be 3 km, below which we linearly extrapolate w_s to zero. We also apply a nudging with a timescale of 6 h towards the initial q_t (total water specific humidity) profile in the free troposphere (above 4 km) to avoid spurious moisture tendencies.

In the trades, vertical shear in the zonal wind component u is most common and to first order set by large-scale meridional temperature gradients through the thermal wind relation:

$$\frac{\partial u_g}{\partial z} \simeq -\frac{g}{fT}\frac{\partial T}{\partial y}, \tag{2}$$

where u_g is the geostrophic zonal wind, T the temperature, g the gravitational acceleration and f the Coriolis parameter. In the northern hemisphere, temperature decreases poleward ($\partial_y T < 0$), so that $\partial_z u_g > 0$, which implies that winds become increasingly westerly (eastward) with height. $\partial_z u > 0$ is indeed typical for most of the year, as derived from ERA5 daily data (12:00 UTC) from 2008 to 2017 within 9°–19° N and 50°–59° W (Fig. 2). In boreal summer, when the ITCZ is located in the northern hemisphere

Table 1. Overview of the various LES experiments on the large (50.4×50.4 km^2) or small domain (12.6×12.6 km^2) and with interactive (constant SST) or fixed surface fluxes. For each set, we differentiate between runs without wind shear (NS), runs with weak (1X), medium (2X) or strong (4X) backward (BS) shear and runs with medium or strong forward (FS) shear (see also Fig. 1d).

Shear		NS	BS			FS	
	accronym		1X	2X	4X	2X	4X
	[10^{-3} s^{-1}]	0.0	+0.9	+1.8	+3.6	−1.8	−3.6
Large domain	interactive surface fluxes	√	√		√		√
	prescribed surface fluxes	√	√		√		√
Small domain	prescribed surface fluxes	√	√	√	√	√	√

and meridional temperature differences within the subtropical belts are smaller, $\partial_z u$ is closer to zero or even negative. Vertical shear in the meridional wind component is close to zero year-round (not shown).

Further analysis of daily profiles (not shown) reveals quite some day-to-day variability in the zonal wind profiles, regardless of the season, with reversals from negative to positive shear or zero shear from one day to the next, or vice versa. Forward shear (here $\partial_z u < 0$) is to some extent a frequent feature of the atmospheric flow in the trades — not only during summer. However, backward shear (here $\partial_z u > 0$) is still the most common.

The magnitude of shear we imposed in our simulations is not far from what we derived from ERA5. We ran simulations with different values for the initial (indicated by the subscript 0) and geostrophic zonal wind profiles ($\partial_z u_0 = \partial_z u_g$), while setting $\partial_z v_0 = \partial_z v_g = 0$. The zonal wind profile has either no shear (NS, solid black line in Fig. 1d), forward shear (FS, $\partial_z u < 0$) or backward shear (BS, $\partial_z u > 0$). The FS and BS simulations have different shear strengths ranging from $|\partial_z u| = 0.9$ km^{-1} (1X, dotted line in in Fig. 1d) over $|\partial_z u| = 1.8$ km^{-1} (2X, dashed lines) to $|\partial_z u| = 3.6$ km^{-1} (4X, solid coloured lines); see also Table 1.

The control simulations were run for two days with interactive surface fluxes, which are parametrised using standard bulk flux formulae:

$$
\begin{aligned}
(\psi w)_s &= -C_S U_1 (\psi_1 - \psi_s), &(3)\\
u_* &= \sqrt{C_M} U_1, &(4)
\end{aligned}
$$

where $\psi \in \{q_t, \theta_l\}$, U is the wind speed, u_* the surface friction velocity, and the subscripts s and 1 stand for the surface values and values on the first model level, respectively. The constants C_S and C_M are the drag coefficients, and they depend on the stability and on the scalar and momentum roughness lengths, which we both set to $z_0 = 1.6 \times 10^{-4}$ m. The drag coefficients are computed following Monin-Obukhov similarity theory (as described in Heus et al., 2010).

We used a domain of $50.4{\times}50.4$ km^2, with a resolution of 100 m in the horizontal directions and doubly periodic boundary conditions. The domain top is at about 18 km and the vertical grid is non-uniform: starting with 10 m at the surface and increasing by a factor of 0.01 at each level to about 190 m at the domain top. In order to evaluate and minimize the effect of different surface winds and surface heat fluxes that develop under shear, we additionally performed simulations with prescribed sensible and latent surface fluxes. We also conducted simulations on a smaller domain ($12.6{\times}12.6$ km^2) where the development of cold pools and deeper clouds is less pronounced (Vogel et al., 2016).

The response to shear is not entirely insensitive to the choice of advection scheme. Here, scalar and momentum advection was performed using a 5th-order advection scheme in the horizontal direction and a 2nd-order advection scheme in the vertical direction. Using a 2nd-order scheme in the horizontal further increased the differences among the shear cases (in particular under free surface fluxes), which we attribute to the fact that the 2nd-order scheme accumulates a lot of energy on the smallest length scales close to the grid size. To reduce horizontal advective errors and allow for a larger time step, the grid was horizontally translated using a velocity that is equal to the imposed wind at 3 km height (Galilean transform, see e.g. Wyant et al., 2018).

3 Impact of shear on cloud- and boundary-layer evolution

We now first focus on the differences in cloud and boundary-layer structure that have developed by the end of a two-day simulation using twelve-hourly averaged profiles (hour 36–48), unless noted otherwise.

3.1 Interactive surface fluxes

Similar to the findings of Brown (1999), who ran simulations for different wind shear on a very small domain (6.4×6.4 km^2), the influence of shear (Fig. 3e–g) on the thermodynamic structure of the boundary layer is overall marginal (Fig. 3a–b), but nonetheless evident in the relative humidity (RH) and cloud fraction profiles (Fig. 3c–d). In the presence of shear, regardless of its direction, cloud fractions above cloud base (approximately 700 m) are larger. In the FS-4X case the layer above 2 km is notably moister, whereas the BS-4X case has a more pronounced decrease of RH (which we interpret as the boundary-layer top) around 2 km. From strong backward to strong forward shear we thus observe a deepening of the moist layer and the disappearance of a pronounced hydrolapse.

Differences in the depth of convection are best seen from the time series of average and maximum cloud top heights (CTH), surface precipitation and low cloud cover, defined as the projected cloud amount from heights up to 4 km (Fig. 4a, c, e, g). Differences in cloud tops start to be pronounced only on day two of the simulations, but looking closer, one can see that the highest cloud tops on day one are that of the FS-4X simulations (in orange). On day two, the NS simulation develops the deepest clouds with even an average cloud top near 7 km, whereas clouds in the simulations with shear, regardless of its sign, remain shallower and rain less. During the final twelve hours clouds in all simulations show a pronounced deepening, and the FS-4X case even takes over from the NS case in terms of cloud tops and rain. Shear apparently inhibits vertical cloud development, but this effect is overall stronger for the BS-4X case than the FS-4X case.

Returning to the time series, we can see that the surface heat fluxes can play a key role in the deepening responses. Heat fluxes diverge very early on in the simulations, whereby the largest and smallest fluxes develop for the FS-4X and BS-4X cases, respectively (Fig. 4m, o). This exemplifies an important and perhaps often overlooked influence of wind shear: Different shear profiles maintain different surface winds through (convective) momen-

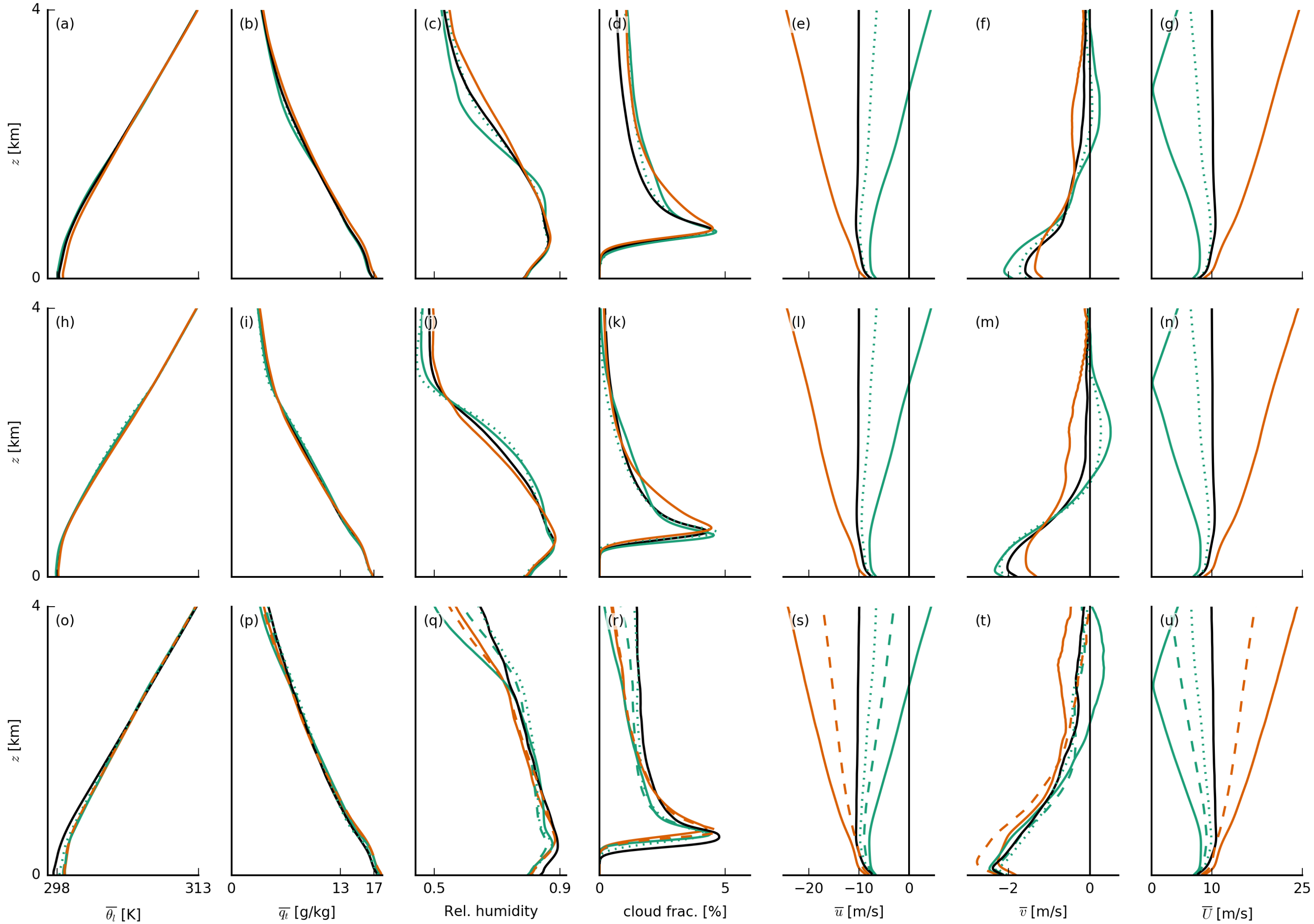

Figure 3. Slab-averaged profiles of thermodynamic quantities of the large-domain simulations with interactive surface fluxes (top row, a-g), with prescribed surface fluxes (middle row, h-n) and small-domain simulations (bottom row, o-u). Shown are averages over the last twelve hours of each simulation of (a, h, o) the liquid water potential temperature θ_l, (b, l, p) total water specific humidity q_t, (c, j, q) relative humidity, (d, k, r) cloud fraction and (e, l, s) zonal, (f, m, t) meridional and (g, n, u) total wind speed, u, v and U, respectively. The line colours and types are explained in Fig. 1 and are the same in all following figures.

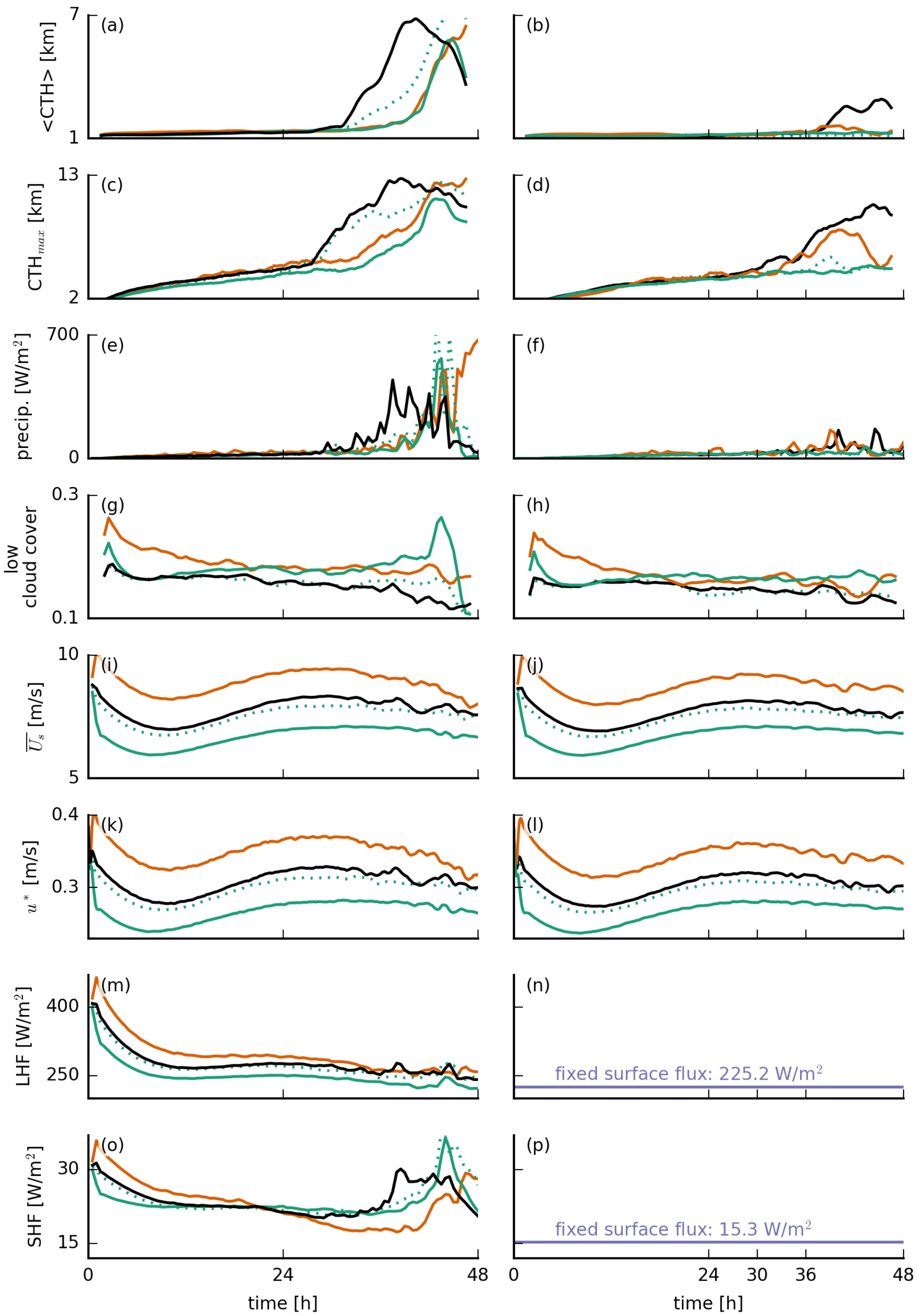

Figure 4. Time series of (a, b) the average and (c, d) the maximum cloud top height (CTH), (e, f) the surface precipitation flux, (g, h) the low cloud cover ($z < 4$ km), (i, j) the domain-averaged total wind speed at 5 m height U_s, (k, l) the surface friction velocity u_*, (m, n) the surface latent heat flux LHF and (o, p) the surface sensible heat flux SHF for the interactive- (left column) and prescribed-surface-flux simulations (right column).

tum transport (Fig. 4i). More specifically, surface winds are stronger under FS than BS (Fig. 4i) due to the mixing of larger zonal wind speeds towards the surface. As this keeps the zonal wind closer to its geostrophic value, there is also less wind turning ($\partial_t v \sim -f(u-u_g)$) and weaker southerly flow (Fig. 3f). These differences in surface winds, in turn, cause differences in surface fluxes.

As clouds deepen in all simulations during day two, the difference in surface heat fluxes becomes smaller, as downward mixing of warm and dry free tropospheric air reduces the surface sensible heat flux while promoting the latent heat flux (Nuijens & Stevens, 2012). The increase in the sensible heat fluxes in the final six hours may be attributed to precipitation and evaporative cooling of rain water in the subcloud layer (e.g. cold pools, Fig. 4e).

3.2 Prescribed surface fluxes

In light of these results, an important question is whether the surface fluxes are the only factor that plays a role in the development of convection, or whether shear has other more direct effects, including on the organization of clouds. Therefore, we carried out simulations with prescribed surface heat fluxes (namely $SHF = 15.3$ W m^{-2} and $LHF = 225.2$ W m^{-2}), which are shown in the right column in Fig. 4 and second row in Fig. 3. Note that the surface friction (or surface momentum flux) is unchanged (Fig. 4k, l).

Apparently, the sensitivity of cloud deepening to shear does not change its overall character when we prescribe the surface heat fluxes. Clouds are overall shallower with lower cloud fractions above 1 km (Fig. 3k, Fig. 4b,d), because the prescribed surface fluxes are smaller than in the interactive flux runs. But the FS-4X case still develops the largest relative humidities above the boundary layer (>2.5 km), whereas the BS-4X case has the most pronounced hydrolapse near the boundary-layer top (Fig. 3j). Again the FS-4X case tends to produce somewhat deeper clouds during day one, but falls behind the NS case on day two. The BS-4X and BS-1X cases remain even shallower.

3.3 Sensitivity to sudden perturbations of shear on a smaller domain

To shed some more light on the role of shear limiting convective deepening, we carried out additional simulations on a 16-fold smaller domain (see Table 1), which is still 4 times as large as the one used by Brown (1999). In these simulations, we followed a

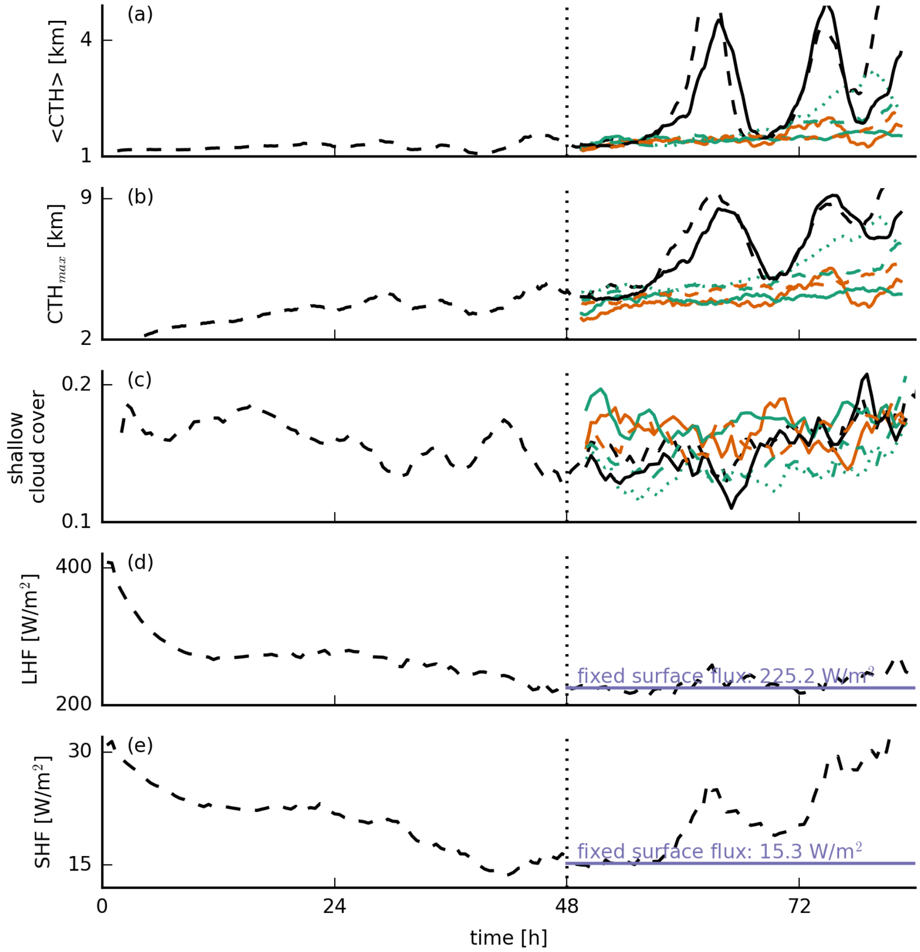

Figure 5. Time series of (a) the average and (b) the maximum cloud top heights (CTH), (c) the low cloud cover ($z < 4$ km) and the (d) surface latent and (e) surface sensible heat fluxes for the small-domain simulations (48–84 h). In addition to the standard line types (see Fig. 1), the dashed black lines indicate a non-sheared simulation with interactive surface fluxes that is used to initialise the simulations at $t = 48$ h by perturbing the wind profiles and fixing the surface fluxes.

slightly different approach because the shallower convection allows the subcloud layer and surface fluxes to reach a steady state after about two days (Fig. 5). Taking the final state of the simulation with no shear (and with interactive surface fluxes, designated by the black dashed line in Fig. 5) we instantaneously perturbed the wind shear as in Fig. 1d, while keeping the surface fluxes constant with the same values as on the large domain. We then let the system evolve for another 36 hours.

When wind shear is introduced, convective deepening is prevented (Fig. 5a–b), which is particularly clear when considering how the simulation develops without perturbation (dashed black line in Fig. 5). Even very weak shear (BS-1X, dashed green line) can effectively reduce cloud depth and delay cloud deepening.

It is worthwhile to compare the profiles of RH and cloud fraction on the small domain (Fig. 3o–u) with those on the large domain. The 16-fold smaller domain leads to much higher relative humidities and cloud fractions above 2 km. This can be explained by the lack of spatial organization of shallow convection on the small domain. Increasing the domain size generally tends to organize the shallow convection into deeper and larger clusters, which leads to a shallower, warmer and drier domain-averaged trade-wind layer (Vogel et al., 2016). Larger domains support stronger and deeper updrafts by allowing them to spread their compensating subsidence over a larger area, which can reduce the effective stability felt by the updraft. On a larger domain the likelihood of developing a strong updraft and deep cloud somewhere may also increase.

In the absence of spatial organization on the small domain, we can observe that only the FS-4X case behaves differently compared to the large domain. This case is no longer comparably moist or even moister than the NS case and its cloud fraction and RH profile is now more in line with that of the BS-4X case. This hints at a role of spatial organization in explaining the response to forward shear, which we address later.

Using the same experimental set-up (i.e. small domain, fixed surface fluxes and sudden perturbation of the wind profile), we carried out some further sensitivity tests in which we applied forward shear to specific layers (Fig. 6). These simulations show that shear is particularly effective in the cloud layer (grey and green lines in Fig. 6), whereas shear in the subcloud layer (pink) or near cloud tops (brown) still leads to cloud deepening.

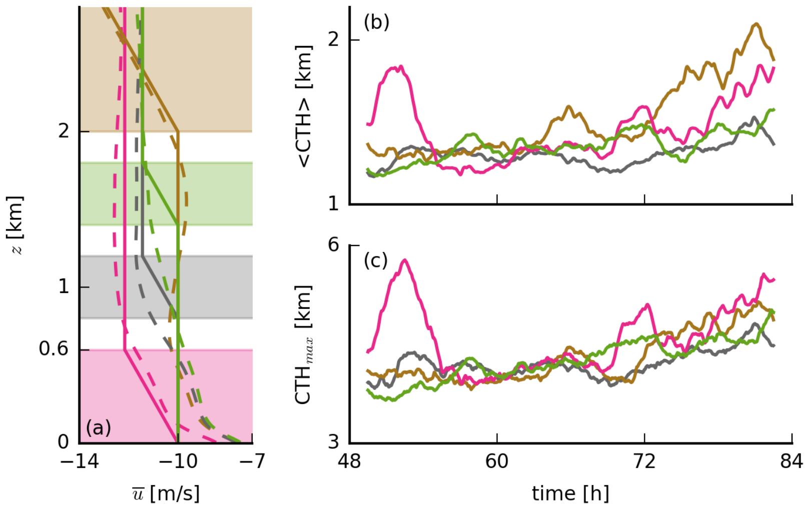

Figure 6. (a) Initial (solid lines) and slab-averaged profiles (from the last twelve hours; dashed lines) of the zonal wind u of simulations in which shear is only applied at limited height levels, as well as (b-c) the corresponding time series of the (b) average and (c) maximum cloud top heights. Pink lines depict the shear at 0–0.6 km, grey at 0.8–1.2 km, green at 1.4–1.8 km and brown at 2–10 km.

3.4 Impact on cloud amount

Having described differences in the cloud fraction profiles with shear above, we now pay specific attention to what explains these differences and to the time series of low cloud cover (Figs. 4g, h and 5c), where low cloud cover is defined as the fraction of vertical columns that have at least one grid box with liquid water below 4 km. As expected, shear enhances the low cloud cover by 10–20 % in both FS and BS simulations where clouds are tilted in the negative and positive x direction, respectively.

Besides the expected impact on cloud cover, there are also some small differences in the cloud fraction profiles — including near cloud base, whose sensitivity has received much attention in recent climate studies (e.g. Vial et al., 2017; Bony et al., 2017). In the presence of shear we observe a slightly larger maximum cloud fraction near cloud base (500–700 m) in the simulations with prescribed surface heat fluxes (Fig. 3d, k). Cloud fraction in the FS-4X case is larger throughout the cloud layer up to 2 km. In the BS-4X this is also true, but less pronounced just above cloud base and extending up to 3 km. In particular in the BS-4X case, the differences within the cloud layer seem to be largely correlated with relative humidities. However, the maximum RH near cloud base is similar in all the simulations. BS-4X has a higher q_t variance at these heights (not shown) which could explain the higher cloud fraction.

The corresponding profile of active cloud fraction, defined as the percentage of cloudy gridpoints with positive buoyancy (not shown), reveals that the larger cloud-base cloud fraction in the BS-4X case (compared to NS) is due to a few percent more active cloud. This is in agreement with a shift in the probability density function (PDF) of subcloud-layer humidity towards larger values, which will be discussed in the next section (Fig. 10, green lines). The FS-4X case has less active cloud fraction, also in agreement with the shift in the humidity PDF towards smaller values. In that simulation, the larger cloud-base cloud fraction is explained by more passive cloud.

4 Sensitivity of convective deepening to shear

Overall, the previous section has shown that the presence of even weak backward shear effectively inhibits convective deepening, while forward shear only slightly weakens the potential to develop deeper clouds. If not through a surface flux response, what is the mechanism through which backward shear oppresses convection, while forward shear seems to allow for cloud deepening? A few ideas, also borrowed from studies of deep convection, are as follows:

1. Wind shear changes the rate of entrainment, the updraft buoyancy and updraft speed: As clouds get tilted through any absolute amount of shear, they may suffer from more lateral entrainment and opposing pressure perturbations that limit updraft speeds and cloud vertical extent.
2. Wind shear changes the structure and organisation of shallow cloud systems. For instance, wind shear may separate regions of updrafts and downdrafts as to help sustain circulations, or it may interact with cold-pool fronts to force stronger updrafts in the subcloud layer.

To investigate these ideas, we consider only the simulations with prescribed surface fluxes and focus on the period between 30 to 36 h (unless noted otherwise), which is when larger differences in the deepening of the clouds first become evident (cf. Fig. 4b, d).

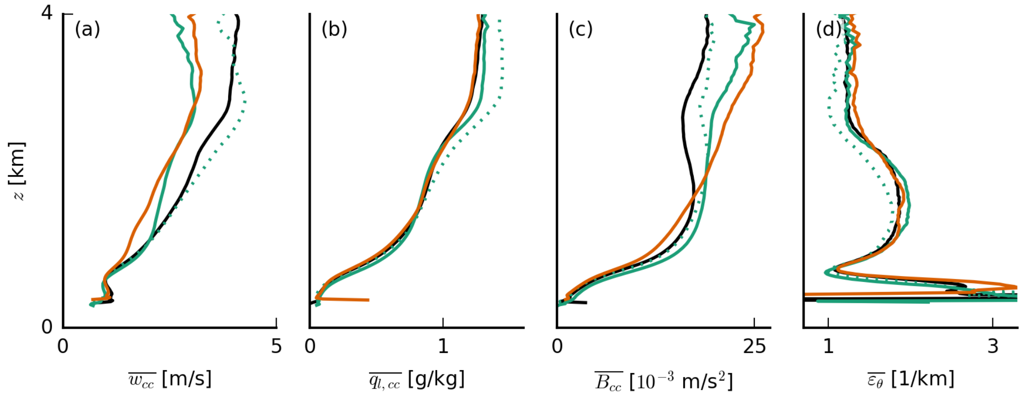

Figure 7. Slab-averaged profiles of (a) the cloud-core vertical velocity w_{cc}, (b) the cloud-core liquid water specific humidity $q_{l,cc}$, (c) the cloud-core buoyancy B_{cc} and (d) the fractional entrainment rate ε_θ of θ_l (averaged from 30 to 36 h of the simulations with prescribed surface fluxes).

4.1 Entrainment and updraft speeds

The FS-4X and BS-4X cases have significantly lower updraft speeds in the cloud cores ($q_l > 0$ and $\theta_v' > 0$) compared to the NS and BS-1X cases (Fig. 7a), which appears key to explaining the lower cloud top heights that develop under shear. However, the strongly sheared simulations contain nearly the same amount of cloud-core liquid water and are notably more buoyant, especially above 2 km (Fig. 7b, c). A similar picture is established if we sample on cloudy points ($q_l > 0$). Buoyancy itself is evidently not key to explaining the weaker updrafts under shear (although it likely explains the stronger updrafts below 1 km in the BS-4X case). The relatively low buoyancy in cloud cores of the NS case (at least above 2 km) is because the environment surrounding the non-sheared clouds is warmer in terms of θ_v (not shown), because clouds in that simulation are already mixing across a deeper layer. Vogel et al. (2016) also showed how quickly the thermodynamic structure of the boundary layer changes as shallow cumuli develop into cumulus congestus.

Using the simple entraining plume model by Betts (1975) to calculate the fractional entrainment rate ε_θ of θ_l (Fig. 7d), we find that clouds in the BS and FS cases entrain only marginally more environmental air if anything (also if we consider entrainment of

q_t, not shown). This suggests that there is no larger lateral entrainment due to shear that could explain weaker vertical development.

The weaker cloud-core vertical velocities under shear are in line with studies of deep convection in squall lines, in particular the recent study by Peters et al. (2019) and earlier work by similar authors (M. D. Parker, 2010; Peters, 2016), who show that slanted updrafts are weaker than upright ones. Peters et al. (2019) decompose the vertical momentum equation into four terms that describe the processes that regulate the vertical acceleration of updrafts: (1) a term associated with momentum entrainment and detrainment, (2) a (downward-oriented) dynamic pressure acceleration term, (3) a (downward-oriented) buoyancy pressure acceleration term and (4) a buoyancy acceleration term (which includes the entrainment of thermodynamic properties that can limit updraft buoyancy). They show that shear mostly enhances the dynamic pressure perturbations, which can be interpreted as an aerodynamic lift force due to the shear-driven cross flow (perpendicular to the direction of ascent). Unlike the lift associated with aircraft wings, the lift in slanted thermals experiencing cross-flow is directed downward. A handful of studies on the vertical velocity budget of shallow convection have also noted a minor role of entrainment in explaining updraft speeds (e.g. de Roode et al., 2012; Romps & Charn, 2015; Morrison & Peters, 2018; Tian et al., 2019).

A deep investigation of the vertical velocity budget — a subject on its own as demonstrated by the aforementioned studies — goes beyond our goal, but we can get an impression of the importance of the pressure perturbations by sampling the vertical velocity budget in cloudy updrafts, following de Roode et al. (2012), here included in Appendix A. We find that the horizontal flux of resolved and subgrid vertical momentum across the cloud boundaries (e.g. entrainment) is important to enhancing the vertical acceleration of the sheared updrafts in the BS-4X and FS-4X cases, but mainly important near cloud base (<1 km), where other tendencies are small. Near cloud tops (> 2 km) updrafts in the sheared runs experience a larger buoyancy force (consistent with Fig. 7c), but also experience a larger negative pressure gradient force that is overall twice as large as the buoyancy force.

A quick look at the total pressure perturbations in x-z cross sections of the NS, BS-4X and FS-4X runs also illustrates that pressure perturbations, especially near the slanted sides and tops of the clouds, are more pronounced under shear (Fig. 8).

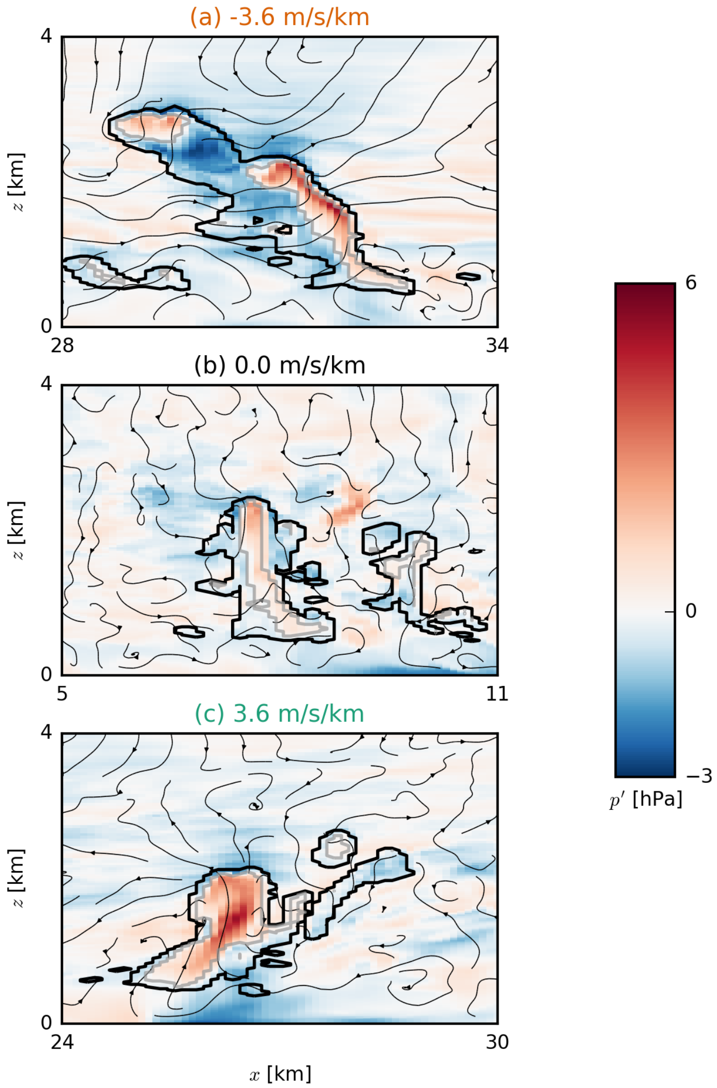

Figure 8. Snapshots of x-z cross sections of the LES domains with (a) FS-4X, (b) NS and (c) BS-4X, showcasing typical circulation and pressure patterns. Plotted are the streamlines of u and w as arrowed lines and the total pressure deviations p' by the colour map (averaged over 500 m in the y direction). The thick black lines indicate clouds and the grey lines indicate cloud cores.

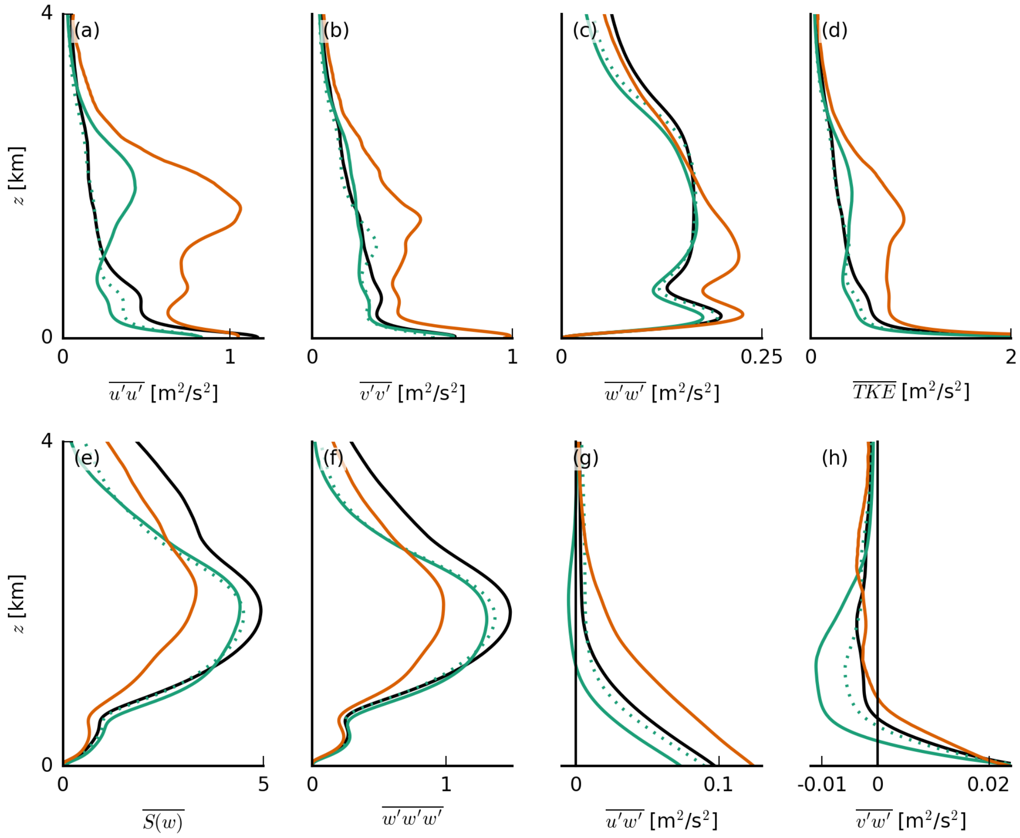

Figure 9. Slab-averaged profiles of the variances of (a) the zonal wind speed $u'u'$, (b) the meridional wind speed $v'v'$ and (c) the vertical velocity $w'w'$, (d) the turbulence kinetic energy (TKE), (e) the skewness $S(w)$, (f) the third moment $w'w'w'$ of the vertical velocity and (g) the zonal and (h) the meridional momentum fluxes, $u'w'$ and $v'w'$, respectively (averaged from 30 to 36 h of the simulations with prescribed surface fluxes).

Overall, our results emphasize that shear keeps clouds shallower by weakening updrafts. However, we also observe that clouds under forward shear have a tendency to get deeper than under backward shear. This is explored next. Furthermore, we investigate the second idea that the structure and organization of turbulence and clouds changes with shear.

4.2 Structure and organization of turbulence and clouds

In Fig. 9 we show a number of quantities that reveal quantitative changes to the character of the turbulence structure of the boundary layer: the domain-averaged variances of the velocity components, the turbulence kinetic energy (TKE), the skewness S and third central moment of the vertical velocity $\overline{w'^3}$ and finally the zonal and meridional momentum fluxes. Velocity variances are clearly enhanced from BS-4X to FS-4X, because the velocity fields can become more heterogeneous when the vertical gradient in wind speed between the surface and cloud tops — the shear — is larger under FS-4X (cf. Fig 3l–n). Consequently, TKE and the momentum fluxes are larger, in agreement with Brown (1999). Momentum fluxes at the surface are largest for the FS-4X case, leading to a larger surface friction (see also Fig. 4i, j) and larger surface layer shear.

Several authors have noted that convection can transition from a closed-cell structure to roll structures due to shear (e.g. Sykes & Henn, 1989; Khanna & Brasseur, 1998; Salesky et al., 2017). A parameter that controls this transition is the ratio of the surface friction velocity u_* to the convective velocity scale w_* (Sykes & Henn, 1989) or equivalently the ratio of the Obukhov length and the boundary-layer height. While the exact value of u_*/w_* at which the transition takes place depends on other properties of the flow (different studies report values between 0.27 and 0.65), low values are clearly associated with cellular convection and high values with roll structures (Fedorovich & Conzemius, 2008; Salesky et al., 2017). In our simulations, u_*/w_* has rather low values, which do not differ greatly among the various shear cases (ranging from about 0.30 for BS-4X to 0.37 for FS-4X), indicating that convection is mainly buoyancy- and not shear-driven in all our simulations.

The skewness of the vertical velocity $S(w) = \overline{w'^3}/\overline{w'^2}^{\frac{2}{3}}$, which is a measure for the asymmetry of the vertical velocity distribution, is reduced with shear, especially when the shear is forward. This is primarily caused by the reduction in the advection of vertical velocity variance, $\overline{w'^3}$ due to on average weaker updrafts into the cloud layer (Fig. 7a). Differences in S and in updraft speeds are much smaller at lower heights. Indeed, PDFs of w at 200 m and at 800 m (near cloud base) in Fig. 10a–b are overall very similar, except that the FS case has notably stronger updrafts as well as stronger downdrafts at both levels, consistent with the larger w variance but smaller skewness (Fig. 9c, e). In addition, the humidity PDFs reveal that the FS-4X case is skewed towards relatively drier values near cloud base (Fig. 10d). This might be a signature of a spatial separation of the downdraft from the updraft region (or alternatively of dry downdrafts, induced by evaporative cooling near the cloud interface). The FS-4X case has the largest absolute amount of wind shear across the subcloud layer, which creates positive (anticlockwise)

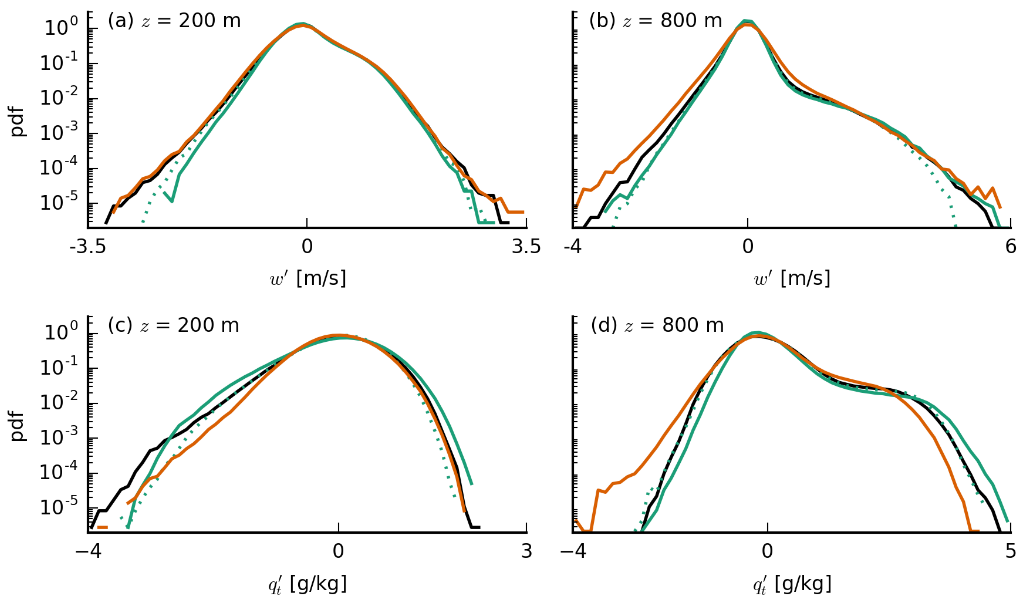

Figure 10. Probability density functions of the vertical velocity w (top) and the total water specific humidity deviations q_t' (bottom) at constant heights of (left) $z = 200$ m and (right) $z = 800$ m (averaged from 30 to 36 h of the simulations with prescribed surface fluxes).

vorticity and may aid the development of stronger circulations that feed moisture into clouds. This broader PDF seems at odds with the larger variance for the FS-4X case at 800 m, but looking closely, the PDF for FS-4X is somewhat wider for vertical velocities between -1 and 1 m/s.

Following the idea of stronger circulations and a difference in the organization of clouds, Fig. 11 shows that the number of clouds near cloud base is larger in the absence of shear, clouds tend to have smaller radii and the moistest areas of the domain get moister with time, while the dry areas get drier. The smaller number of clouds in the FS-4X and BS-4X cases (Fig. 11b) may be an indication that it is harder for moist thermals to reach their LCL when subjected to shear. At the same time, the FS-4X and the NS cases develop the largest clouds (Fig. 11a). As the maximum cloud radius of the FS-4X and NS cases increases during episodes of deeper convection (around 40 h), the number of clouds accordingly decreases, which shows that large clustered clouds are responsible for the deepening of the cloud field. The formation or aggregation of deeper cloud clusters is also evident from the moisture field. Fig. 11c shows deviations of the vertically integrated moist static energy within blocks of 12.6×12.6 km^2 compared to the domain mean, and com-

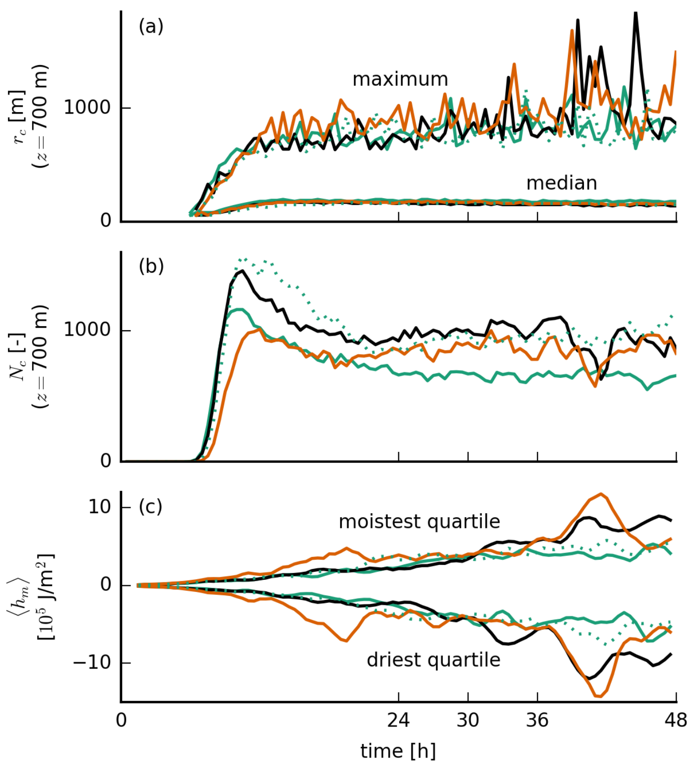

Figure 11. Time series of (a) the median and maximum cloud radius r_c at $z = 700$ m, (b) the number of clouds N_c at that height and (c) the vertically integrated moist static energy anomalies $\langle h_m \rangle$ in the moistest and the driest quartiles of 12.6×12.6 km^2 blocks for the simulations with prescribed surface fluxes.

pares the moistest and the driest quartiles of the domain (in terms of total water path), which is a common measure for self-aggregation (Bretherton & Blossey, 2017). This reveals the strongest moistening of the moist regions and strongest drying of the dry regions in the NS and FS-4X cases. During the first simulation day, this is even most pronounced for the FS-4X case.

We can further support the idea that shear distorts moisture aggregations by investigating snapshots of the moisture field (Fig. 12) from episodes of deep convection: They show that large patches of high or low moisture are much more common in the absence of shear compared to the simulations with shear. We remark that an elongation of structures is not apparent, which is in line with the above discussion that our shear does not cause a transition to rolls. Though large organised structures can occur in all our simulations simply due to the size of our domain, the visual inspection suggests that

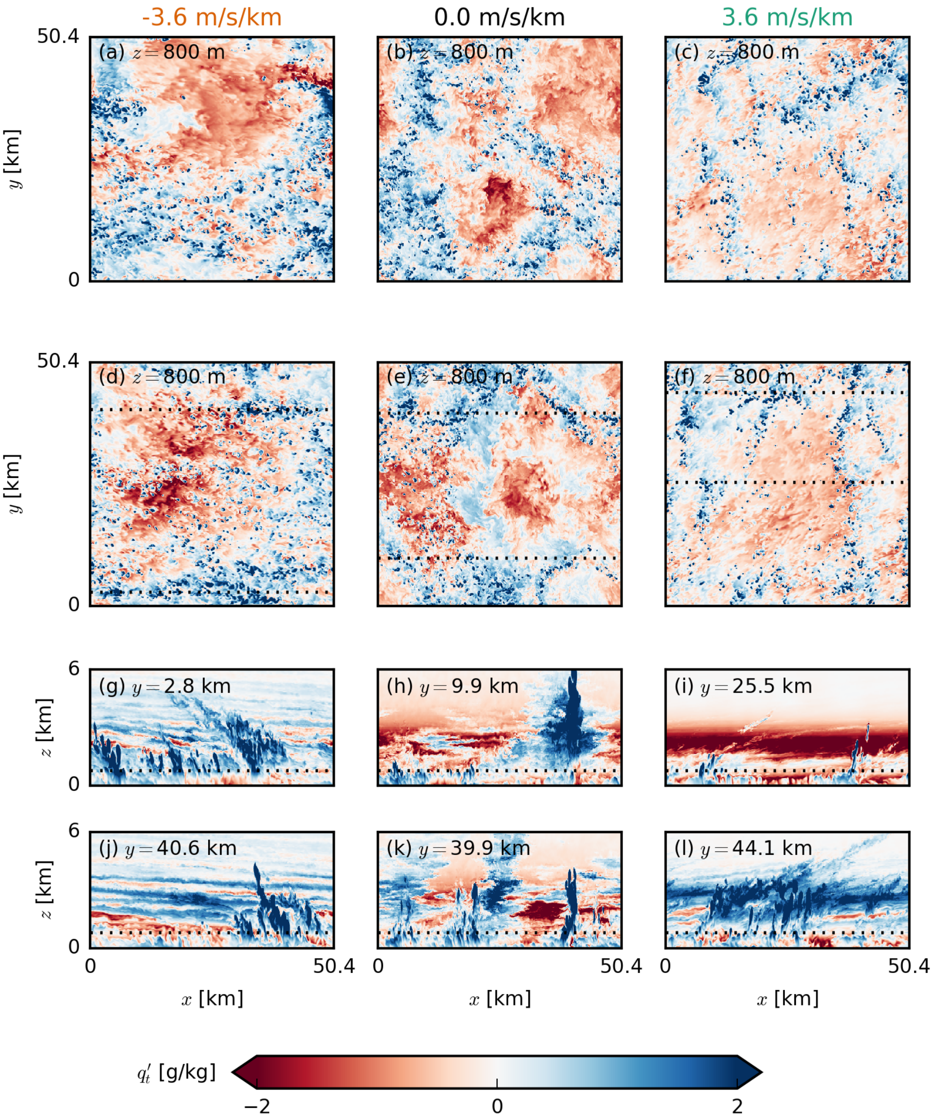

Figure 12. Snapshots of the LES domains of FS-4X (left), NO (centre) and BS-4X (right) exhibiting typical characteristics in the late stages of the simulations. The top two rows (a-f) show horizontal x-y cross sections at two times ($t = 39.0$ h and $t = 46.5$ h) near cloud base ($z = 800$ m) of the deviations from the mean of the total water specific humidity q_t'. The bottom two rows (g-l) show corresponding vertical x-z cross sections from the lowest 6 km of the domain of the latter of the two times (d-f). The horizontal dotted lines indicate the position of the respective other cross sections.

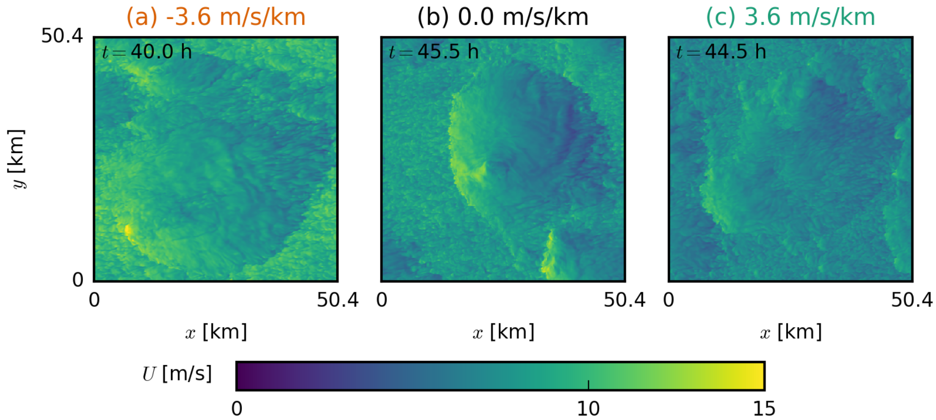

Figure 13. Snapshots of the LES domains of (a) FS-4X, (b) NO and (c) BS-4X exhibiting typical characteristics of the total wind speed U in the late stages of the simulations with prescribed surface fluxes. Shown are horizontal x-y cross sections at $z = 5$ m.

they are most common for NO (when they are also least disturbed), still quite usual for FS-4X and rather rare for BS-4X (in line with Fig. 11). Note that on the smaller domain such aggregations occur much less commonly and nearly exclusively in the absence of shear, underlining the fact that it is such aggregations that allow clouds to grow deep in the presence of forward shear.

Thus, the presence of forward shear helps to promote cloud development through enhanced moisture aggregation and stronger circulations (as measured by the strength of updrafts and downdrafts). Backward shear instead appears to slow down moisture aggregation and the formation of larger cloud clusters, as compared to having no shear. Exactly why the FS-4X and NS cases develop larger, stronger updrafts and more pronounced moisture aggregation compared to the BS-4X case is still subject to further study. A few ideas to be tested include the interaction of clouds with environmental vorticity and the role of cold pools, which upon interacting with the environmental shear can trigger force-lifted updrafts (e.g. Li et al., 2014). However, because convective deepening already differs between the various simulations at stages where precipitation is still limited (see Fig. 4d and f), we believe that the latter mechanism comes second at explaining differences in cloud height and aggregation. Nonetheless, intrigued by the fact that the momentum transported downward through precipitating downdrafts differs depending on wind shear and can change local cold-pool wind characteristics (Fig. 13), we will explore the relative roles of the dynamic and cold-pool effects on convective initiation under shear in a follow-up study.

5 Conclusions

In this paper, we have shown that wind shear strongly influences the depth and characteristics of shallow cumulus convection. Using idealised large-eddy simulations representative of the trades, we have demonstrated that even weak vertical shear in the zonal wind component can retard the growth of cumulus clouds, in particular when the shear vector is directed against the mean wind direction (backward shear). Furthermore, we have shown that shear increases the cloud fraction independent of the surface fluxes — an effect that has been of major interest in recent climate studies (e.g. Vial et al., 2017; Bony et al., 2017).

Backward shear, whereby surface easterlies become upper westerlies, are typical for the winter trades, presumably because this season has a larger meridional temperature gradient between the equator and subtropics, which via the thermal wind equation is linked to zonal wind shear. ERA5 data for the North Atlantic trades also shows pronounced day-to-day variability in zonal wind shear. For instance, weak shear and forward shear (easterlies become stronger with height) are not uncommon during boreal winter, even if they are more typical for boreal summer when the ITCZ and deep convection shift northward.

Simulations with interactive surface fluxes reveal that backward shear can slow down vertical cloud development by influencing the surface wind speed via momentum transport. Under backward shear relatively weaker wind speeds are mixed towards the surface compared to a no-shear or a forward-shear wind profile. Although our simulations are forced with the same geostrophic wind at the surface, the weakest surface winds develop under backward shear. This in turn leads to weaker surface heat fluxes. Under backward shear, mean cloud tops remain near 2 km for at least 36 hours of simulation, at which point the simulations without (imposed) shear have developed clouds with mean tops near 7 km.

The vertical development of clouds under forward shear is also delayed, but not as much as with backward shear, because simulations with forward shear develop the strongest surface winds and (initially) the largest surface heat fluxes. To elucidate more direct effects of the absolute amount of wind shear, we repeated the simulations with prescribed surface heat fluxes. These show that the presence of absolute shear in the cloud layer limits updraft speeds, in line with studies of deep convection that have shown shear to inhibit convective development (e.g. Peters et al., 2019). Entrainment plays a minor role in setting the weaker updrafts (e.g. de Roode et al., 2012; Romps & Charn, 2015; Morrison & Peters, 2018; Tian et al., 2019). Instead, both forward and backward shear leads to a larger downward pressure perturbation force that weakens vertical accelerations.

In addition, shear changes the turbulence structure of the subcloud layer. Though our simulations remain buoyancy-driven and do not develop roll structures or cloud streets, shear is found to influence the development of aggregated moist regions and stronger updrafts and downdrafts. Moisture aggregation and the development of large cloud clusters is more pronounced under forward shear and smallest under backward shear, leading to similarly deep convection under forward shear as in the absence of it. An explanation may be sought in the amount of shear in the subcloud layer, which remains largest under forward shear. This can separate the downdrafts from the updrafts, and the associated background vorticity may help develop stronger mesoscale circulations or even interact with cold pool boundaries to create forced uplift (Li et al., 2014). This will be the subject of a further study.

As clouds remain shallower under backward shear, the moistening of the cloud layer is more pronounced and the top of the cloud layer is marked by a steeper decrease in humidity, as is typical near the trade-wind inversion (e.g. Riehl et al., 1951). The moister subcloud and cloud layer, as well as a stronger inversion, will lead to more cloudiness. Therefore, we may argue that the trade-wind inversion largely owes its name to the effect of the trade-winds in keeping convection shallow and that backward shear is a crucial ingredient in defining the typical trade-wind-layer structure.

Appendix A Impact of shear on the vertical-velocity budget

We follow the approach from de Roode et al. (2012) to compute the vertical-velocity budget of cloudy updrafts. In Figure A1, we present this budget in the form the same form as Eq. 5 of de Roode et al. (2012)

$$\frac{\partial w_c}{\partial t} = \underbrace{\frac{g(\theta_{v,c} - \overline{\theta_v})}{\theta_0}}_{B} - \underbrace{\frac{1}{2}\frac{\partial w_c^2}{\partial z}}_{A} - \underbrace{\left[\frac{\partial \pi}{\partial z}\right]_c}_{P} - \underbrace{\frac{1}{\sigma_c}\frac{\partial \sigma_c \overline{w''w''}^c}{\partial z}}_{Subpl.} - \underbrace{\frac{\epsilon_w w_c^2}{1-\sigma_c}}_{Entr.} + \underbrace{f u_c}_{C}, \tag{A1}$$

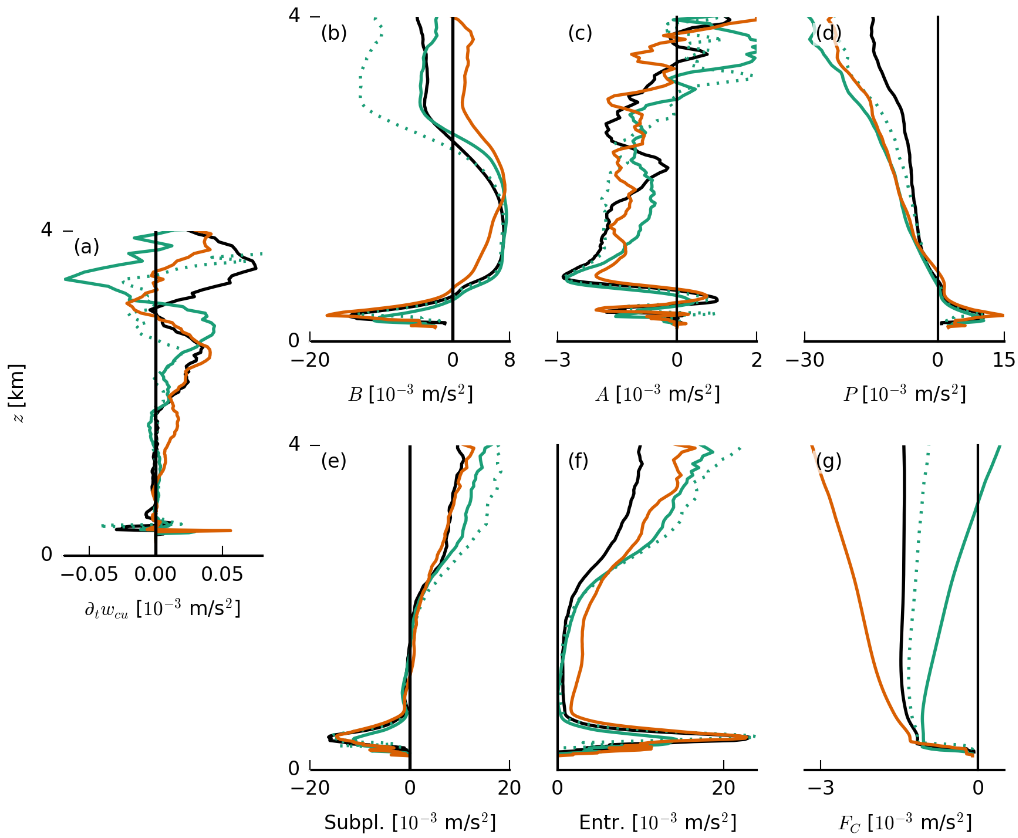

Figure A1. Slab-averaged profiles (averaged from 30 to 36 h of the simulations with prescribed surfaces fluxes) of the terms of the cloudy-updraft vertical velocity budget (Eq. A1).

where the subscript c stands for conditional sampling (here: on cloudy updrafts, i.e. $q_l > 0$ and $w > 0$), g the gravitational acceleration, θ_v the virtual potential temperature, θ_0 a reference temperature, π the modified pressure, σ the area fraction and ϵ_w the fractional entrainment rate of w. We stress that this budget uses the modified pressure, which is defined as

$$\pi = \frac{1}{\rho_0}\left(p - \overline{p_h}\right) + \frac{2}{3}e, \tag{A2}$$

where ρ_0 is a constant reference density, p the pressure, p_h the hydrostatic pressure and e the subgrid-scale TKE. The latter is included because in DALES, $\frac{2}{3}e$ is subtracted from the subgrid momentum flux to simplify its computation; to compensate for this, the term is added back to the pressure (Heus et al., 2010). Therefore, one needs to be careful when interpreting the pressure term in the vertical-velocity budget as differences may be due to differences in the subgrid TKE.

Nonetheless, we would like to point out that the pressure term is somewhat stronger (negative) at greater heights in the presence of shear in this budget. Some of this is compensated by the entrainment term, which is stronger (positive) with shear. Given that the entrainment term is calculated from the residual and following the above line of arguments, this is expected if we assume that the differences in the pressure term are solely due to subgrid TKE differences. Furthermore, it is striking that the pressure term is much stronger than the buoyancy term. However, the differences in the entrainment term are somewhat larger than those in the pressure term, suggesting that they are not solely due to subgrid TKE differences. This makes us confident to deduce that indeed shear leads to stronger negative pressure deviations near cloud tops, which reduce updraft speeds (in line with Peters et al., 2019).

Acknowledgments

We would like to thank Chris Bretherton and Bjorn Stevens for stimulating discussions. This project has received funding from the European Research Council (ERC) under the European Union's Horizon 2020 research and innovation programme (Starting grant agreement no. 714918). DALES is open-source software, which is distributed under the terms of the GNU GPL version 3. The exact version of the code as well as the input files used in this work are available via `https://doi.org/10.5281/zenodo.3714862`.

References

Asai, T. (1970). Three-dimensional features of thermal convection in a plane Couette flow. *Journal of the Meteorological Society of Japan. Ser. II*, *48*(1), 18–29.

Bellon, G., & Stevens, B. (2012). Using the Sensitivity of Large-Eddy Simulations to Evaluate Atmospheric Boundary Layer Models. *Journal of the Atmospheric Sciences*, *69*(5), 1582–1601. doi: 10.1175/JAS-D-11-0160.1

Betts, A. K. (1975). Parametric Interpretation of Trade-Wind Cumulus Budget Studies. *Journal of the Atmospheric Sciences*, *32*(10), 1934–1945. doi: 10.1175/1520-0469(1975)032⟨1934:PIOTWC⟩2.0.CO;2

Bony, S., & Dufresne, J.-L. (2005). Marine boundary layer clouds at the heart of tropical cloud feedback uncertainties in climate models. *Geophysical Research Letters*, *32*(20). doi: 10.1029/2005GL023851

Bony, S., Stevens, B., Ament, F., Bigorre, S., Chazette, P., Crewell, S., … Wirth, M. (2017). EUREC4A: A Field Campaign to Elucidate the Couplings Between Clouds, Convection and Circulation. *Surveys in Geophysics*. doi: 10.1007/s10712-017-9428-0

Bony, S., Stevens, B., Held, I. H., Mitchell, J. F., Dufresne, J.-L., Emanuel, K. A., … Senior, C. (2013). Carbon Dioxide and Climate: Perspectives on a Scientific Assessment. In G. R. Asrar & J. W. Hurrell (Eds.), *Climate Science for Serving Society* (pp. 391–413). Dordrecht: Springer Netherlands. doi: 10.1007/978-94-007-6692-1_14

Bretherton, C. S., & Blossey, P. N. (2017). Understanding Mesoscale Aggregation of Shallow Cumulus Convection Using Large-Eddy Simulation. *Journal of Advances in Modeling Earth Systems*, *9*(8), 2798–2821. doi: 10.1002/2017MS000981

Brown, A. R. (1999). Large-eddy simulation and parametrization of the effects of shear on shallow cumulus convection. *Boundary-Layer Meteorology*, *91*(1), 65–80.

Brueck, M., Nuijens, L., & Stevens, B. (2015). On the Seasonal and Synoptic Time-Scale Variability of the North Atlantic Trade Wind Region and Its Low-Level Clouds. *Journal of the Atmospheric Sciences*, *72*(4), 1428–1446. doi: 10.1175/JAS-D-14-0054.1

Daleu, C. L., Woolnough, S. J., & Plant, R. S. (2012). Cloud-Resolving Model Simulations with One- and Two-Way Couplings via the Weak Temperature Gradient Approximation. *Journal of the Atmospheric Sciences*, *69*(12), 3683–3699. doi: 10.1175/JAS-D-12-058.1

de Roode, S. R., Siebesma, A. P., Jonker, H. J. J., & de Voogd, Y. (2012). Parameterization of the Vertical Velocity Equation for Shallow Cumulus Clouds. *Monthly Weather Review*, *140*(8), 2424–2436. doi: 10.1175/MWR-D-11-00277.1

Fedorovich, E., & Conzemius, R. (2008). Effects of wind shear on the atmospheric convective boundary layer structure and evolution. *Acta Geophysica*, *56*(1), 114–141. doi: 10.2478/s11600-007-0040-4

Grabowski, W. W. (1998). Toward Cloud Resolving Modeling of Large-Scale Tropical Circulations: A Simple Cloud Microphysics Parameterization. *Journal of* *the Atmospheric Sciences*, *55*(21), 3283–3298. doi: 10.1175/1520-0469(1998)055⟨3283:TCRMOL⟩2.0.CO;2

Heus, T., van Heerwaarden, C. C., Jonker, H. J. J., Siebesma, P. A., Axelsen, S., van den Dries, K., ... Vilà-Guerau de Arellano, J. (2010). Formulation of the Dutch Atmospheric Large-Eddy Simulation (DALES) and overview of its applications. *Geoscientific Model Development*, *3*(2), 415–444. doi: 10.5194/gmd-3-415-2010

Hildebrand, P. H. (1998). Shear-Parallel Moist Convection over the Tropical Ocean: A Case Study from 18 February 1993 TOGA COARE. *Monthly Weather Review*, *126*(7), 1952–1976. doi: 10.1175/1520-0493(1998)126⟨1952:SPMCOT⟩2.0.CO;2

Hill, G. E. (1968). On the orientation of cloud bands. *Tellus*, *20*(1), 132–137. doi: 10.3402/tellusa.v20i1.9936

Khanna, S., & Brasseur, J. G. (1998). Three-Dimensional Buoyancy- and Shear-Induced Local Structure of the Atmospheric Boundary Layer. *Journal of the Atmospheric Sciences*, *55*(5), 710–743. doi: 10.1175/1520-0469(1998)055⟨0710:TDBASI⟩2.0.CO;2

Klein, S. A., Hall, A., Norris, J. R., & Pincus, R. (2017). Low-Cloud Feedbacks from Cloud-Controlling Factors: A Review. *Surveys in Geophysics*, *38*(6), 1307–1329. doi: 10.1007/s10712-017-9433-3

Koren, I., Remer, L. A., Altaratz, O., Martins, J. V., & Davidi, A. (2010). Aerosol-induced changes of convective cloud anvils produce strong climate warming. *Atmos. Chem. Phys.*, *10*(10), 5001–5010.

LeMone, M. A., & Pennell, W. T. (1976). The Relationship of Trade Wind Cumulus Distribution to Subcloud Layer Fluxes and Structure. *Monthly Weather Review*, *104*(5), 524–539. doi: 10.1175/1520-0493(1976)104⟨0524:TROTWC⟩2.0.CO;2

Li, Z., Zuidema, P., & Zhu, P. (2014). Simulated Convective Invigoration Processes at Trade Wind Cumulus Cold Pool Boundaries. *Journal of the Atmospheric Sciences*, *71*(8), 2823–2841. doi: 10.1175/JAS-D-13-0184.1

Malkus, J. S. (1949). Effects of wind shear on some aspects of convection. *Transactions, American Geophysical Union*, *30*(1), 19. doi: 10.1029/TR030i001p00019

Malkus, J. S. (1963). Cloud Patterns over Tropical Oceans. *Science*, *141*(3583), 767–778. doi: 10.1126/science.141.3583.767

Morrison, H., & Peters, J. M. (2018). Theoretical Expressions for the Ascent Rate of Moist Deep Convective Thermals. *Journal of the Atmospheric Sciences*, *75*(5), 1699–1719. doi: 10.1175/JAS-D-17-0295.1

Nuijens, L., & Stevens, B. (2012). The Influence of Wind Speed on Shallow Marine Cumulus Convection. *Journal of the Atmospheric Sciences*, *69*(1), 168–184. doi: 10.1175/JAS-D-11-02.1

Park, S.-B., Böing, S., & Gentine, P. (2018). Role of Surface Friction on Shallow Nonprecipitating Convection. *Journal of the Atmospheric Sciences*, *75*(1), 163–178. doi: 10.1175/JAS-D-17-0106.1

Parker, D. J. (1996). Cold pools in shear. *Quarterly Journal of the Royal Meteorological Society*, *122*(535), 1655–1674. doi: 10.1256/smsqj.53508

Parker, M. D. (2010). Relationship between System Slope and Updraft Intensity in Squall Lines. *Monthly Weather Review*, *138*(9), 3572–3578. doi: 10.1175/2010MWR3441.1

Pastushkov, R. S. (1975). The effects of vertical wind shear on the evolution of convective clouds. *Quarterly Journal of the Royal Meteorological Society*, *101*(428), 281–291. doi: 10.1002/qj.49710142811

Peters, J. M. (2016). The Impact of Effective Buoyancy and Dynamic Pressure Forcing on Vertical Velocities within Two-Dimensional Updrafts. *Journal of the Atmospheric Sciences*, *73*(11), 4531–4551. doi: 10.1175/JAS-D-16-0016.1

Peters, J. M., Hannah, W., & Morrison, H. (2019). The Influence of Vertical Wind Shear on Moist Thermals. *Journal of the Atmospheric Sciences*, *76*(6), 1645–1659. doi: 10.1175/JAS-D-18-0296.1

Riehl, H., Yeh, T. C., Malkus, J. S., & La Seur, N. E. (1951). The north-east trade of the Pacific Ocean. *Quarterly Journal of the Royal Meteorological Society*, *77*(334), 598–626.

Robe, F. R., & Emanuel, K. A. (2001). The Effect of Vertical Wind Shear on Radiative–Convective Equilibrium States. *Journal of the Atmospheric Sciences*, *58*(11), 1427–1445. doi: 10.1175/1520-0469(2001)058⟨1427:TEOVWS⟩2.0.CO;2

Romps, D. M., & Charn, A. B. (2015). Sticky Thermals: Evidence for a Dominant

Balance between Buoyancy and Drag in Cloud Updrafts. *Journal of the Atmospheric Sciences*, *72*(8), 2890–2901. doi: 10.1175/JAS-D-15-0042.1

Rotunno, R., Klemp, J. B., & Weisman, M. L. (1988). A Theory for Strong, Long-Lived Squall Lines. *Journal of the Atmospheric Sciences*, *45*(3), 463–485. doi: 10.1175/1520-0469(1988)045⟨0463:ATFSLL⟩2.0.CO;2

Salesky, S. T., Chamecki, M., & Bou-Zeid, E. (2017). On the Nature of the Transition Between Roll and Cellular Organization in the Convective Boundary Layer. *Boundary-Layer Meteorology*, *163*(1), 41–68. doi: 10.1007/s10546-016-0220-3

Sathiyamoorthy, V., Pal, P. K., & Joshi, P. C. (2004). Influence of the Upper-Tropospheric Wind Shear upon Cloud Radiative Forcing in the Asian Monsoon Region. *Journal of Climate*, *17*(14), 2725–2735. doi: 10.1175/1520-0442(2004)017⟨2725:IOTUWS⟩2.0.CO;2

Sykes, R. I., & Henn, D. S. (1989). Large-Eddy Simulation of Turbulent Sheared Convection. *Journal of the Atmospheric Sciences*, *46*(8), 1106–1118. doi: 10.1175/1520-0469(1989)046⟨1106:LESOTS⟩2.0.CO;2

Thorpe, A. J., Miller, M. J., & Moncrieff, M. W. (1982). Two-dimensional convection in non-constant shear: A model of mid-latitude squall lines. *Quarterly Journal of the Royal Meteorological Society*, *108*(458), 739–762. doi: 10.1002/qj.49710845802

Tian, Y., Kuang, Z., Singh, M. S., & Nie, J. (2019). The Vertical Momentum Budget of Shallow Cumulus Convection: Insights From a Lagrangian Perspective. *Journal of Advances in Modeling Earth Systems*, *11*(1), 113–126. doi: 10.1029/2018MS001451

Vial, J., Bony, S., Stevens, B., & Vogel, R. (2017). Mechanisms and Model Diversity of Trade-Wind Shallow Cumulus Cloud Feedbacks: A Review. *Surveys in Geophysics*, *38*(6), 1331–1353. doi: 10.1007/s10712-017-9418-2

Vogel, R., Nuijens, L., & Stevens, B. (2016). The role of precipitation and spatial organization in the response of trade-wind clouds to warming. *Journal of Advances in Modeling Earth Systems*, *8*(2), 843–862. doi: 10.1002/2015MS000568

Weisman, M. L., & Rotunno, R. (2004). "A Theory for Strong Long-Lived Squall Lines" Revisited. *Journal of the Atmospheric Sciences*, *61*, 361–382.

Wyant, M. C., Bretherton, C. S., & Blossey, P. N. (2018). The Sensitivity of Numerical Simulations of Cloud-Topped Boundary Layers to Cross-Grid Flow. *Journal of Advances in Modeling Earth Systems*, *10*(2), 466–480. doi: 10.1002/2017MS001241